communications physics

Article

https://doi.org/10.1038/s42005-024-01871-8

Wobbling and migrating ferrofluid droplets

Check for updates

Aaveg Aggarwal[1], Shih-Yuan Chen[2], Eleftherios Kirkinis[1], Mohammed Imran Khan[3], Bei Fan[3], Michelle M. Driscoll[2] & Monica Olvera de la Cruz[1,2,4,5]

Active components incorporated in materials generate motion by inducing conformational changes in response to external fields. Magnetic fields, in particular, carry the added advantage of biocompatibility as well as being able to actuate materials remotely. Although ferrofluid droplet migration induced by a high-frequency rotating magnetic field is a well-established effect, droplet migration at low frequencies is still elusive. Millimeter-sized ferrofluid droplets placed on a solid substrate, surrounded by an ambient gas phase, are shown here to migrate under a rotating magnetic field due to inertia-induced symmetry-breaking of the periodic deformation (wobbling) of the liquid-gas interface. This interface wobbling leads to droplet migration with speeds that increase as the amplitude and frequency of the magnetic field increase. In addition to migrating in a controlled manner, we demonstrate the ability of magnetic droplets to clean surface impurities and transport cargo.

Soft active materials are characterized by their dynamic response to external stimuli. Unlike passive materials, active materials have the ability to respond to different inputs such as light[1–3], magnetic fields[4,5], electric fields[6,7], and chemical cues[8–10]. Active components incorporated in passive materials enable controlled conformational changes to achieve specific functions such as migration, swimming, and delivering cargo. Moreover, soft materials actuated by magnetic fields hold significant appeal due to the fact that magnetic fields can penetrate a wide range of materials, including biological matter.

Ferrofluids are colloidal suspensions of magnetic nanoparticles that can be actuated using external magnetic fields. Since the motion of magnetic particles inside the host fluid can generate macroscopic fluid flow, the magnetic fields enable tunable fluid control in situ without changing the fluid properties and confinement. Different actuation schemes can be devised to manipulate magnetic liquids. Ferrofluids and other magnetic materials have been explored to achieve locomotion via spatial gradients in magnetic fields. These gradients can be established by using magnets[11] or current-carrying coils[12]. The magnetic field source can also be physically moved[13] or periodically turned off and on[14], to create fields with spatio-temporal variations.

Rotating magnetic fields have also been used to actuate matter for robotic applications[15,16]. For ferrofluid droplets, this approach relies on the rotating field-generated fluid motion leading to actuation of the droplet as a whole. Although the individual magnetic constituents of the ferrofluid experience no net force in a spatially uniform external field, the magnetic particles rotate to align with the field and drag the surrounding fluid along, causing macroscopic fluid motion[17,18].

Rotational fields have been used to drive ferrofluid droplets in liquid environment[19], pattern and control the moving direction of a pack of ferrofluid droplets[20], and to direct ferrofluid droplets along magnetic rails[21]. High frequency rotating fields can create internal torques in ferrofluids causing the fluid to rotate along with the field[22–24]. This phenomenon can also be used to displace ferrofluid droplets on solid substrates[18] as the droplet fluid develops internal rotations.

While the relation between contact angle and capillary number or contact angle versus time are well established in the literature of spreading of viscous liquids by fitting curves to macroscopic measurements[25], the microscopic physics near the contact line is still a topic of current investigation[26,27]. Likewise, there hasn't been any real consensus on the magnetowetting properties of ferrofluids. There are many reasons why this is the case. For instance, the carrier liquid plays a significant role, where oil-based ferrofluids give rise to a free-surface protrusion while under identical conditions magnetic paints give rise to a dimple (the Moses effect)[28]. The diverse properties of ferrofluid wetting behavior were collected in a number of recent reviews[29,30].

In this work, we show numerically and verify experimentally, that in the regime of negligible torques (no internal rotations), ferrofluid droplets on a solid substrate surrounded by an ambient gas phase, can migrate by applying an external rotating magnetic field. The liquid-gas interface deforms in the direction of the magnetic field[24], whose circulation causes the droplet and its contact lines to wobble. We find that this geometric wobbling of the droplet and its interaction with the solid substrate, causes the droplets to migrate. While previous studies have observed droplet motion induced by symmetry breaking through mechanical vibration[31,32], our discovery intro-

[1]Department of Materials Science and Engineering, Northwestern University, Evanston, IL, USA. [2]Department of Physics and Astronomy, Northwestern University, Evanston, IL, USA. [3]Department of Mechanical Engineering, Michigan State University, East Lansing, MI, USA. [4]Department of Chemistry, Northwestern University, Evanston, IL, USA. [5]Department of Chemical and Biological Engineering, Northwestern University, Evanston, IL, USA. e-mail: m-olvera@northwestern.edu

duces a method to drive droplet motion via active self-vibration, eliminating the need for a mechanically actuated substrate. In the ensuing sections, we develop a finite element analysis model to study the magnetically-induced deformation and motion of these droplets. The accompanying experimental realization of magnetic droplets in a rotating magnetic field, then verifies the overall trend of the numerical predictions.

Results and discussion

Ferrofluids are incompressible suspensions of nanosize ferromagnetic particles in a viscous carrier liquid. When internal rotations are neglected, their dynamical behavior is determined by the Navier-Stokes equations $\rho D_t v_i = -\partial_i p + \eta \partial_j^2 v_i + f_i$, where D_t is the convective derivative, v_i is the i-th component of liquid velocity, p the pressure, ρ density, η the dynamic viscosity and f_i is the i-th component of an external force. All magnetic effects are described by a magnetic force given by the magnetic stress tensor[24]

$$\boldsymbol{\sigma}_{\mathrm{m}} = -\mu_0 \left\{ \int_0^H M(H) dH + \frac{1}{2} H^2 \right\} \mathbf{I} + \mathbf{BH}. \tag{1}$$

Here, $\mathbf{M}$ is the fluid macroscopic magnetization, $\mathbf{H}$ is the magnetic field, and $\mathbf{B}$ is the magnetic flux density satisfying $\nabla \times \mathbf{H} = 0$ and $\nabla \cdot \mathbf{B} = 0$, respectively and the magnetization is given by eq. (3). μ_0 is the magnetic susceptibility in vacuum and $\mathbf{I}$ is the identity tensor. We use bold symbols to denote vectors and tensors, and non-bold symbols for their respective magnitudes.

In stating eq. (1) we have tacitly assumed that the magnetization relaxation time is very small, thus the magnetization is collinear with the magnetic field at all times. In addition, the system is isothermal and the magnetization only depends on the field amplitude H, leading the magnetic body force per unit volume (that is, the divergence of eq. (1)) to vanish[24]. However, the magnetic traction entering the interfacial normal stress condition

$$[[\mathbf{n} \cdot \boldsymbol{\sigma}_{\mathrm{m}} \cdot \mathbf{n}]] \equiv \mu_0 \int_0^H M dH + \frac{1}{2} \mu_0 (\mathbf{M} \cdot \mathbf{n})^2 = p + 2\mathcal{K}\gamma, \tag{2}$$

is *non-zero*, causing a commensurate geometric deformation of the liquid-gas interface. Here, $[[\cdot]]$ denotes the jump in the field across the interface of the droplet, $\mathbf{n}$ is the unit normal vector to the liquid-gas interface pointing outwards, γ is surface tension, $\mathcal{K}$ the mean curvature and $\mathbf{M} = \frac{M}{H}\mathbf{H}$. The fields $\mathbf{H}$ and $\mathbf{B}$ satisfy analogous jump conditions at an interface. Figure 1a shows a finite element simulation that demonstrates the effect of the normal stress condition (eq. (2)) at an interface by employing a ferrofluid droplet suspended in air. The interface of the droplet becomes elongated along the direction of the magnetic field, while at the same time it is stabilized by surface tension.

A ferrofluid droplet placed on a solid substrate also experiences the same magnetic force and undergoes a similar elongation. To test this, we use a commercial water-based ferrofluid (FerroTec, EMG 700) and deposit a droplet of the fluid with ~ 1.5 mm radius on a chemically-coated hydrophobic glass slide (see "Experimental method" subsection in the Methods section for more details). A schematic representation of the experimental setup is shown in Fig. 1b. The droplet is then exposed to a magnetic field pointing in the $+z$ direction. Figure 2a shows the droplet geometries in the

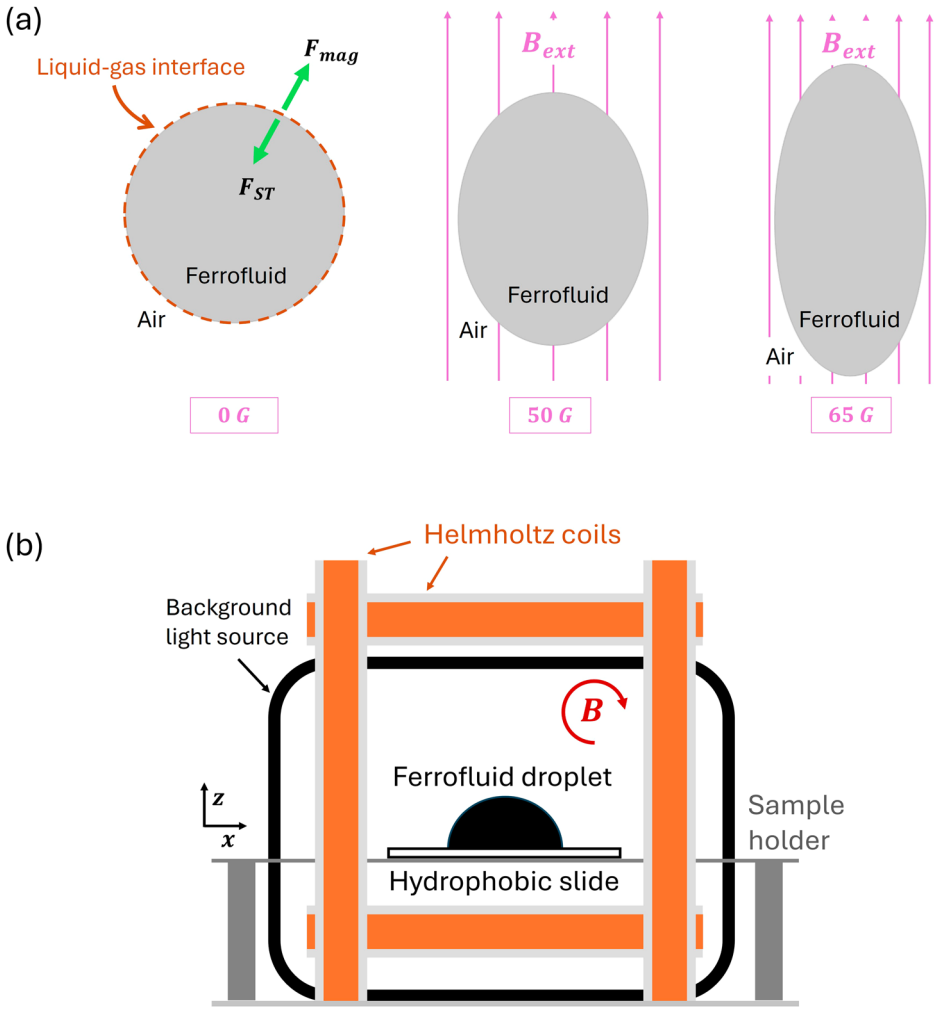

Fig. 1 | Ferrofluid in magnetic field. a Finite element simulation of a ferrofluid droplet suspended in air in the presence of three different external magnetic field magnitudes B_{ext}, that is, 0 G (left), 50 G (middle) and 65 G (right). The geometry of the liquid-gas interface is determined by the balance between the magnetic interfacial force (F_{mag}) and its surface-tension (F_{ST}) counterpart. **b** A schematic representation of the experimental setup where the Helmholtz coils are used to actuate magnetic droplets placed in the center. See Supplementary Fig. 1 for a photograph of the Helmholtz coils used for the experiments.

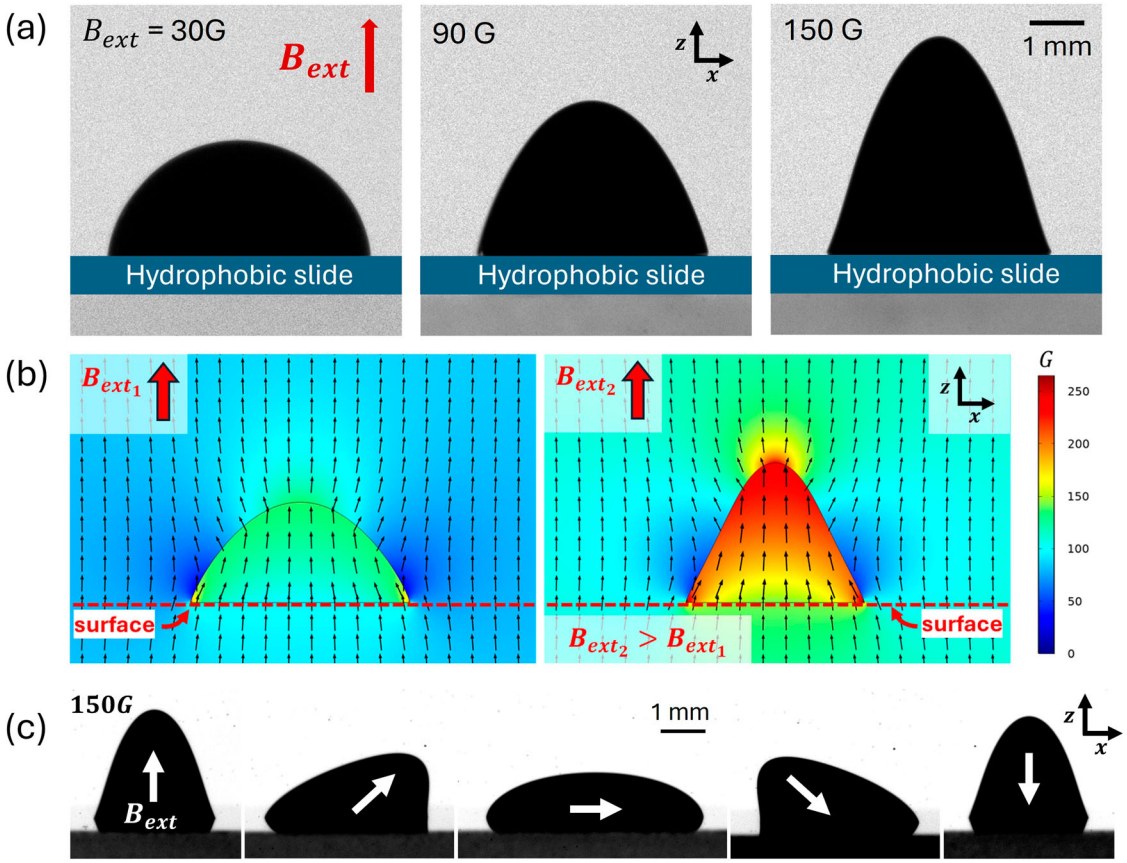

Fig. 2 | Deformation of the droplet interface due to magnetic field. a Photographs from experiments demonstrating an increase in the peak height of the ferrofluid droplet with an increase in the external field strength, B_{ext}. Magnetic fields used here are 30 G, 90 G, and 150 G, and the field points in the $+z$ direction (scale bar = 1 mm). **b** Finite element model simulating the deformation of a 2D ferrofluid droplet as a function of increasing magnetic field strength. The location of the hydrophobic slide is here denoted with the horizontal red dashed line (surface). **c** Experimentally observed stationary steady state configurations acquired by a ferrofluid droplet under uniform and unidirectional external magnetic fields at various angles indicated by white arrows (scale bar = 1 mm).

presence of three different external field strengths, that is, 30 G, 90 G and 150 G respectively, demonstrating an increase in the droplet's deformation with an increasing magnetic field strength.

This behavior can be described by the Navier-Stokes equations in conjunction with the additional magnetic force (eq. (2)). We can thus calculate the droplet geometries as a function of magnetic field amplitude. Fig. 2b displays the droplet deformation in the presence of different magnetic fields pointing upwards along the z-axis, calculated using the finite element method. The model shows the dependence of the droplet's peak height on the amplitude of the magnetic field. Furthermore, due to the nature of the magnetic force, the interface tilts in the direction of the external magnetic field. In panel (c) of Fig. 2, we display the experimental realization of this tilt where the droplet is exposed to a uniform and unidirectional external field at various angles indicated using white arrows. To achieve this tilted geometry, the contact lines of the droplet move until they reach a steady stationary state. Due to this phenomenon, the droplet displays an apparent "wobble" in the presence of a magnetic field rotating in the $x-z$ plane (see Supplementary Movie 1). The droplet wobbles at twice the frequency of the rotating field due to the squared force term in eq. (2); that is, if the magnetization of the droplet $\boldsymbol{M}$ rotates at an angular frequency ω, the magnetic force rotates at 2ω.

The placement of the droplet on a solid substrate creates a pair of contact angles between the liquid-gas and liquid-solid interfaces. The mobility of the contact lines is a critical factor in determining the motion of the whole droplet. It is experimentally known that contact lines can become pinned whenever the dynamic contact angles $\theta(t)$ lie within a finite interval $\Theta_R < \theta(t) < \Theta_A$ of their static receding and advancing counterparts, (see Fig. 3a). This phenomenon, known as contact angle hysteresis, occurs due to surface roughness, chemical contamination and other microscopic interactions of the surface with the fluid. The substrate used in the experiments (Fig. 2c) has a contact angle hysteresis of roughly 15°, that is, $\Theta_A - \Theta_R \approx 15°$. The wobbling motion of the droplet causes both contact angles of the droplet to oscillate (see Supplementary Movie 1). This allows the pinned contact lines of the droplet to overcome contact angle hysteresis and become unpinned (cf. Fig. 3a(*i*)-(*ii*)). The incipient motion of both contact lines over a full cycle of rotation of the magnetic field causes the droplet to become displaced relative to its initial position, thereby inducing migration. The direction of the droplet migration follows the same 'sense' as the magnetic field, that is, the droplet moves along the positive x-axis for a field rotating clockwise in the x-z plane, and vice-versa. Using the finite element analysis model, we observe this property of ferrofluid droplets to migrate due to periodic wobbling of the interface (see Supplementary Movie 2). Fig. 3b shows the simulated motion of a 2-dimensional droplet via chronologically arranged snapshots. Here, the color bar shows the magnitude of fluid velocity in the interior of the droplet (see "Experimental method" subsection in the Methods section for material parameters used in the model), and the black arrows point in the instantaneous direction of the magnetic field. The model is in qualitative agreement with the motion observed in the laboratory (see Supplementary Movie 3). Fig. 3c shows experiments where the migration of the droplet was induced using an external magnetic field (indicated using white arrows) of 100 G rotating at 10 Hz.

In the Stokes-flow regime (no inertia) and on a perfectly smooth substrate, during the first half of the deformation cycle, a wobbling droplet would deform into a sequence of geometric conformations that are mirror images (about y-z plane) of the conformations during the second half. Therefore, under such conditions, the droplet should symmetrically move

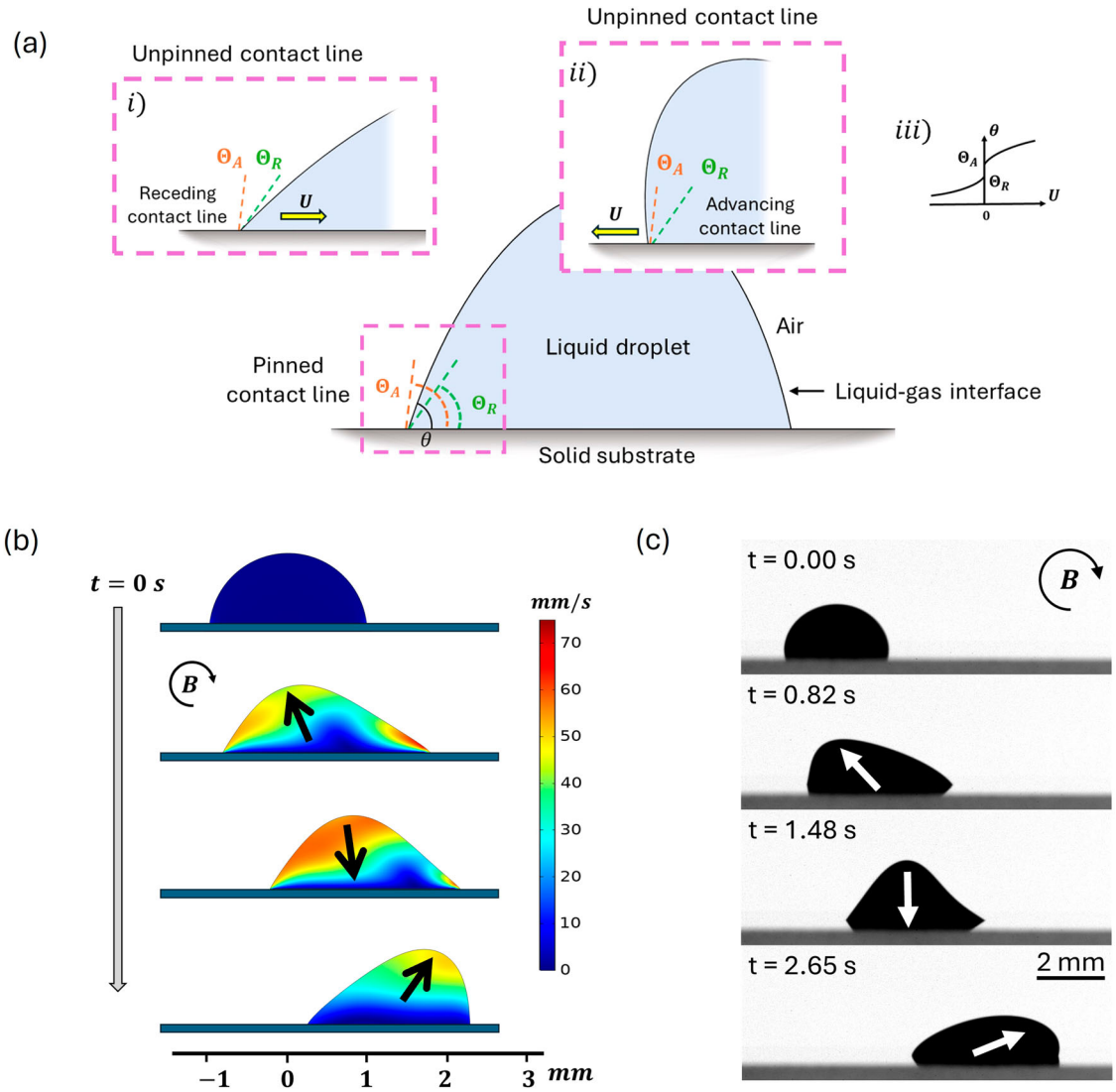

Fig. 3 | Migration of ferrofluid droplets in rotating fields. a A schematic representation of contact angle pinning. Insets (*i*) & (*ii*): representation of receding and advancing contact lines. (*iii*): Schematic depiction of contact angle hysteresis diagram (contact line velocity U vs. the dynamic contact angle θ, adopted from[39]). **b** Finite element simulations demonstrating the migration of a 2D droplet due to the wobbling motion of the liquid-gas interface. The magnetic field is rotating clockwise at 10 Hz in the $x-z$ plane. Black arrows indicate the instantaneous direction of the external magnetic field (see Supplementary Movie 2). **c** Experimental photographs of a ferrofluid droplet undergoing the motion predicted by the finite element model, displayed in panel (**b**). White arrows indicate the instantaneous direction of the external magnetic field (scale bar = 2 mm).

back and forth such that after every cycle, it returns back to the original position (also see Supplementary Note 2). This symmetry of the forward and backward motions is broken in our system due to the inertia of the fluid flow inside the droplet. The fluid flow depends on the amplitude and frequency of the magnetic field and therefore can be used to control the speed of the droplet motion. Figure 4 displays the droplet speed as a function of field frequency for three different values of field amplitudes, that is, 50 G, 100 G and 150 G, demonstrating an increase in the droplet speed with an increase in the field amplitude and frequency. Each data point in the plot is an average of five separate experiments using a new droplet on a clean glass substrate and the standard deviation of the measurements are plotted as error bars. A noteworthy feature of Fig. 4 is the existence of a critical frequency for a given field amplitude below which the droplet is immobile. This is because, for the contact lines to become unpinned and move, the wobbling of the droplet interface needs to be large enough to overcome contact angle hysteresis. Therefore, for a smaller value of field amplitude, a larger critical frequency is required to set the droplet in motion. As shown in Fig. 4, for the field amplitudes of 150 G and 100 G, the critical frequencies are approximately 5 Hz and 7 Hz respectively, and for 50 G, the droplet stayed immobile for the whole range of frequencies tested as wobble could not unpin the contact lines. In our experiments, we also noticed that sometimes the contact lines would become unpinned and move back and forth while the overall droplet stayed immobile. This phenomenon was captured in the Supplementary Movie 1. One explanation for this phenomenon is the variation in surface roughness which can cause a moving contact line to get pinned as it moves to a different part of the substrate. This was confirmed by the different values taken by the contact angle hysteresis interval, measured at different positions on the glass substrate. Moreover, as the field frequency or the amplitude was raised, the droplet was able to freely move over the entire substrate. The droplet motion is also affected by parameters such as droplet size and fluid's material properties. For example, for a given magnetic field amplitude, smaller sized droplets wobble much less compared to larger droplets, which causes them to stay pinned on the substrate and not move. This expected behavior was observed in both simulations and experiments.

By controlling the axis of rotation of the magnetic field we can manoeuvre the droplets in any arbitrary direction on a solid substrate and in

addition they can be induced to travel up or down inclined planes. The droplets can also interact with materials that lie along the path of their motion. This ability of the droplets can be used to clean surface impurities, harvest materials, and transport matter to desired locations on the substrate's surface. To demonstrate this functionality, we deposit a ferrofluid droplet at the bottom of a curved Teflon substrate, and place a small cube of a soft PEGMEA-based hydrogel (cargo) near the droplet (see Fig. 5a). We drive the droplet uphill in the direction of the cargo using a magnetic field of 125 G rotating counterclockwise at 10 Hz until the droplet overruns the cargo (see Fig. 5b–d). This allows the droplet to pick up and move the cargo along with it. We then flip the direction of the field rotation to clockwise causing the droplet and cargo to move downhill together as shown in Fig. 5e–g (also see Supplementary Movie 4). This shows our ability to control the motion of ferrofluid droplets on complex surfaces and also use them to transport matter.

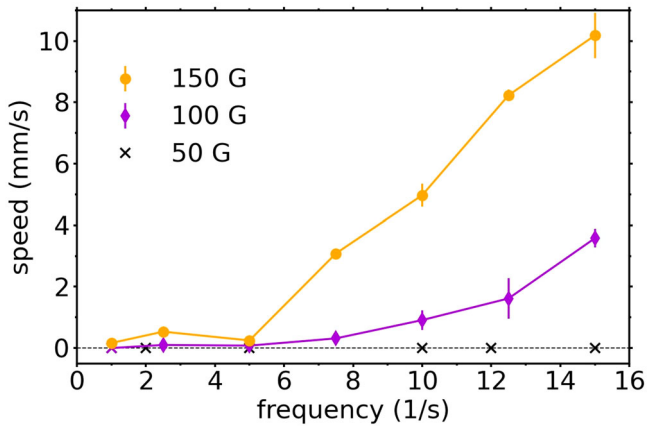

Fig. 4 | Experimental measurements of ferrofluid droplet migration speeds on a solid substrate surrounded by an ambient gas phase as a function of the rotating magnetic field frequency. The data points represent an average of five experiments at respective magnetic field amplitudes and the error bars are the standard deviations. Onset of droplet motion takes place at higher frequencies when the field amplitude is lower. This is the case because, for the contact lines to become unpinned and move, the wobbling of the droplet interface needs to be large enough to overcome contact angle hysteresis. Thus, for each field amplitude, a critical frequency exists below which the droplet is immobile.

The model can also be used to analyse the motion of the droplet under different environmental conditions. For example, our numerical calculations show that for surfaces with large contact angle hysteresis ($\Theta_A - \Theta_R \sim 50°$) and low surface tension, the droplet moves in the opposite 'sense' relative to the magnetic field circulation, that is, droplets travel in negative x direction for a field rotating clockwise in the $x - z$ plane (see Supplementary Movie 5, parameters used are given in "Experimental method" section). This reversed motion is associated with the inability of the right contact line to overcome the large hysteresis in the first half stroke of the clockwise rotating cycle. However, synchronization of the second half stroke with the fluid back-flow towards the left contact line, leads the latter to overcome hysteresis effects and sets the droplet into motion.

Conclusions

In this article, we demonstrated a mechanism by which droplets of magnetic liquids can be manipulated over a solid substrate using rotating magnetic fields. In the regime of negligible torques (no internal rotations), a ferrofluid droplet can move via the deformation of its liquid-gas interface and broken symmetry due to inertia. The rotation of the magnetic field creates periodic deformations in the droplet interface causing it to wobble. The wobbling interface creates fluid flows inside the droplet and inertia of the fluid leads the droplets to migrate. The speed of droplet motion is controlled by the amplitude and frequency of the magnetic field. The droplets move in the same sense relative to the magnetic field rotation, that is, the droplets displace in the positive x direction for a clockwise rotating field. We demonstrate this phenomenon of droplet motion through finite element modeling and experiments performed using water-based ferrofluid placed on a hydrophobic substrate.

The finite element model allows us to explore different range of environmental and material parameters inaccessible to our experimental

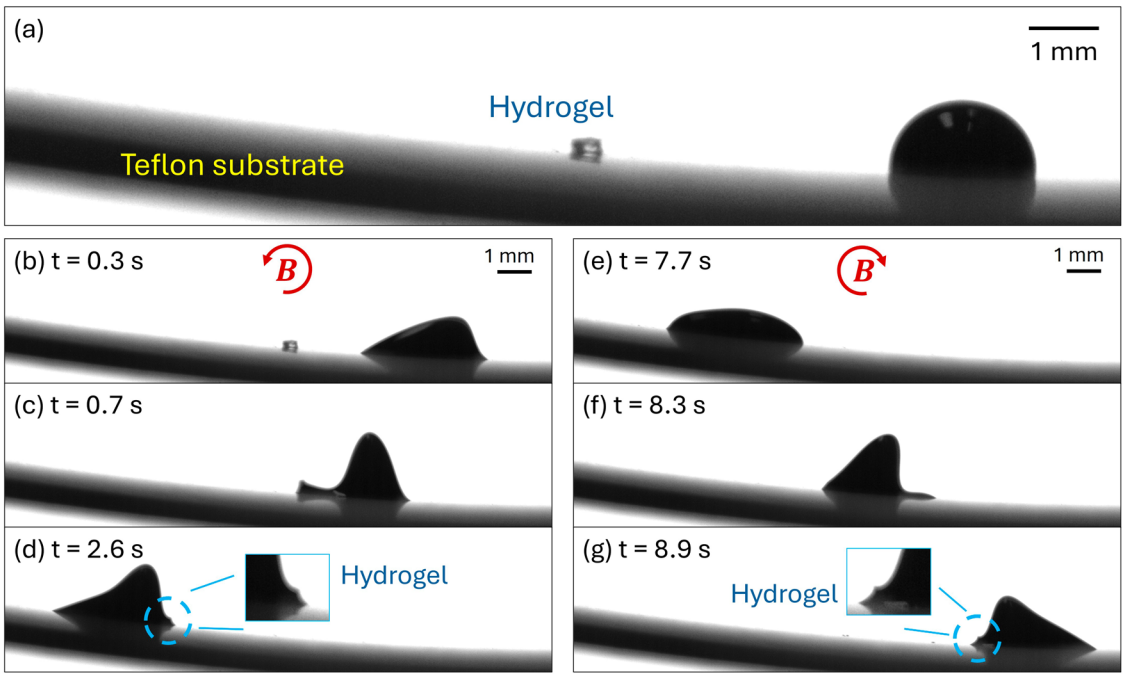

Fig. 5 | Experimental photographs of ferrofluid droplet picking up and transporting cargo. a Photograph showing the initial state of the droplet and cargo. **b–d** Chronologically arranged images of the ferrofluid droplet as it moves up an inclined plane to pick up the cargo. **e–g** Chronologically arranged images of the ferrofluid droplet as it moves down the inclined plane to deliver the cargo. (scale bar = 1 mm).

system. For instance, the model predicts that for substrates with large contact angle hysteresis, the droplets move in the opposite sense relative to the magnetic field rotation. Our work can also be extended to theoretically analyze more complex systems such as oil-based ferrofluid droplets in aqueous environments[33] as well as to explore functions such as cleaning surface impurity, interacting with complex geometry like curved surfaces, dragging matter, and delivering cargo.

Methods

Experimental method

We use a commercial ferrofluid (FerroTec, EMG 700, fluid density $\rho = 1290$ kg/m^3, viscosity $\mu = 5$ cP, surface tension $\gamma = 51$ mN/m[34], saturation magnetization $M_s = 355$ G, receding static contact angle $\Theta_R = 75°$, advancing static contact angle $\Theta_A = 90°$) and quantify the contact angle hysteresis of the ferrofluid on the hydrophobic surface with a drop shape analyzer (Krüss, DSA100). We first deposit a ferrofluid droplet on a clean, hydrophobic slide while the other side of the droplet remains attached to a synringe needle. We then gradually increase the droplet volume (0.5 μL/s) and measure the advancing contact angle when the contact line is sliding both along the substrate and the needle. We then decrease the drop volume ($-$ 0.5 μL/s) and measure the receding contact angle. The reported static advancing angle is 90° and the receding angle is 75°. We further check the inhomogeneity of the substrate properties by depositing ferrofluid droplets at different locations on the substrate, and apply a DC field to stretch the droplet against the gravity. As the droplet deforms, we observe that it develops a strong pinned contact line in some locations while not in others. To minimize the pinned contact line problem, we only perform experiments in locations with less variation in substrate properties, e.g., where we observe no pinned contact line. (All details on the instruments and materials used are given in the Supplementary Note 1).

Computational method

To solve the continuum model we used a commercial finite element analysis software, COMSOL Multiphysics[35]. The computational model comprises of a square box of area 14 mm × 14 mm to model the ambient gas phase which encloses a small semi-spherical domain of radius 1 mm representing the ferrofluid droplet. External magnetic field is applied to the square boundary of the air domain using the condition, $\boldsymbol{n} \cdot \boldsymbol{B} = \boldsymbol{n} \cdot \boldsymbol{B}_{external}$, where $\boldsymbol{n}$ is the normal to the boundary and $\boldsymbol{B}_{external}$ is the external magnetic flux density. Our model utilizes COMSOL's AC/DC module to solve for the magnetic fields and the computational fluid dynamics module to solve the Navier-Stokes equations with magnetic force applied at the droplet interface. The droplet is modeled using the *moving mesh* method defined within the framework of Arbitrary Lagrangian-Eulerian (ALE) formulation[36], where the fluid-air interface is described as a geometric surface and the interfacial forces are directly applied on the boundary of the fluid domain. The advantage of using the moving mesh method is that it provides a very sharp and accurate interface.

Here, we consider the case of very small relaxation time of the magnetization, which is thus collinear with the magnetic field (quasi-stationary theory, cf.[24]). In this case the magnetization is described by the Langevin function

$$M(H) = M_s\left(\coth(\tau H) - \frac{1}{\tau H}\right), \quad \tau = \frac{m_d}{k_B T}, \tag{3}$$

where, $M_s = n m_d$ is the saturation magnetization, $m_d = M_d V$ is the magnetic moment of a single subdomain particle, V is the particle volume, M_d is the domain magnetization of dispersed ferromagnetic material and n is the number density of the magnetic grains. The magnetic force is then described by eq. (2).

We implemented contact angle hysteresis using the approach developed by Cai and Song[37]. On a perfectly smooth surface with no contact angle hysteresis, the liquid-gas interface of a viscous droplet at rest makes an angle θ_{eq} with the surface. This angle is determined by the balance of interfacial forces given by the Young-Laplace equation[38]. If the dynamic contact angle of the droplet differs from θ_{eq}, the contact line moves until θ and θ_{eq} are equal. In order to implement contact angle hysteresis, θ_{eq} is changed depending upon whether the contact line is in a *pinned state* or an *unpinned state*[37]. In the *pinned state* where $\Theta_R \le \theta \le \Theta_A$, the energy of the liquid-solid interface is constantly adjusted such that, $\theta_{eq} = \theta$. This causes the contact lines to become stationary. On the other hand, when the dynamic contact angle exceeds the static advancing angle, that is, $\theta > \Theta_A$, we fix $\theta_{eq} = \Theta_A$. In this case, since the dynamic contact angle exceeds the equilibrium contact angle, the contact lines are free to move. Similarly, when $\theta < \Theta_R$, we fix $\theta_{eq} = \Theta_R$.

The material parameters used in the model (Fig. 3b and Supplementary Movie 2) are fluid density $\rho = 1290$kg/m^3, viscosity $\mu = 5$ cP, surface tension $\gamma = 51$ mN/m, saturation magnetization $M_s = 355$ G, receding static contact angle $\Theta_R = 75°$, advancing static contact angle $\Theta_A = 90°$.

Parameters used in Supplementary Movie 5 are fluid density $\rho = 1290$kg/m^3, viscosity $\mu = 10$ cP, surface tension $\gamma = 30$ mN/m, saturation magnetization $M_s = 355$ G, receding static contact angle $\Theta_R = 55°$, advancing static contact angle $\Theta_A = 110°$.

Data availability

All data are presented in the main text and Supplementary Information. Data files are available upon request.

Code availability

COMSOL simulation files are available upon request.

Received: 20 June 2024; Accepted: 11 November 2024;
Published online: 26 November 2024

References

1. Aggarwal, A., Li, C., Stupp, S. I. & de la Cruz, M. O. Controlling the shape morphology of origami-inspired photoresponsive hydrogels. *Soft matter* **18**, 2193–2202 (2022).
2. Zhao, Y. et al. Soft phototactic swimmer based on self-sustained hydrogel oscillator. *Sci. Robot.* **4**, eaax7112 (2019).
3. Palacci, J. érémie, Sacanna, S., Vatchinsky, A., Chaikin, P. M. & Pine, D. J. Photoactivated colloidal dockers for cargo transportation. *J. Am. Chem. Soc.* **135**, 15978–15981 (2013).
4. Driscoll, M. & Delmotte, B. Leveraging collective effects in externally driven colloidal suspensions: Experiments and simulations. *Curr. Opin. colloid interface Sci.* **40**, 42–57 (2019).
5. Jackson, B. A., Terhune, K. J. & King, L. B. Ionic liquid ferrofluid interface deformation and spray onset under electric and magnetic stresses. *Phys. Fluids*. **29**, 064105 (2017).
6. Zhang, B., Yuan, H., Sokolov, A., de la Cruz, M. O. & Snezhko, A. Polar state reversal in active fluids. *Nat. Phys.* **18**, 154–159 (2022).
7. Pradillo, G. E., Karani, H. & Vlahovska, P. M. Quincke rotor dynamics in confinement: rolling and hovering. *Soft Matter* **15**, 6564–6570 (2019).
8. Li, S., Matoz-Fernandez, D. A., Aggarwal, A. & de la Cruz, M. O. Chemically controlled pattern formation in self-oscillating elastic shells. *Proc. Natl Acad. Sci.* **118**, e2025717118 (2021).
9. Maeda, S., Hara, Y., Sakai, T., Yoshida, R. & Hashimoto, S. Self-walking gel. *Adv. Mater.* **19**, 3480–3484 (2007).
10. Manna, R. K., Shklyaev, O. E. & Balazs, A. C. Chemically driven multimodal locomotion of active, flexible sheets. *Langmuir* **39**, 780–789 (2023).
11. Sarkhosh, M. H., Yousefi, M., Bijarchi, M. A., Nejat, P. H. & Forghani, K. Manipulation of ferrofluid marbles and droplets using repulsive force in magnetic digital microfluidics. *Sens. Actuators A: Phys.* **363**, 114733 (2023).
12. Nguyen, N.-T., Beyzavi, A., Ng, K. M. & Huang, X. Kinematics and deformation of ferrofluid droplets under magnetic actuation. *Microfluidics Nanofluidics* **3**, 571–579 (2007).

13. Nguyen, N.-T., Zhu, G., Chua, Y.-C., Phan, V.-N. & Tan, S.-H. Magnetowetting and Sliding Motion of a Sessile Ferrofluid Droplet in the Presence of a Permanent Magnet. *Langmuir* **26**, 12553–12559 (2010).
14. Fan, X., Dong, X., Karacakol, A. C., Xie, H. & Sitti, M. Reconfigurable multifunctional ferrofluid droplet robots. *Proc. Natl Acad. Sci.* **117**, 27916–27926 (2020).
15. Li, C. et al. Fast and programmable locomotion of hydrogel-metal hybrids under light and magnetic fields. *Sci. Robot.* **5**, eabb9822 (2020).
16. Li, M., Pal, A., Byun, J., Gardi, G. & Sitti, M. Magnetic putty as a reconfigurable, recyclable, and accessible soft robotic material. *Adv. Mater.* **35**, 2304825 (2023).
17. Kirkinis, E. Magnetic torque-induced suppression of van-der-Waals-driven thin liquid film rupture. *J. Fluid Mech.* **813**, 991–1006 (2017).
18. Aggarwal, A., Kirkinis, E. & de la Cruz, M. O. Activity-induced migration of viscous droplets on a solid substrate. *J. Fluid Mech.* **955**, A10 (2023).
19. Sun, M., Hao, B., Yang, S., Wang, X., Majidi, C. & Zhang, L. Exploiting ferrofluidic wetting for miniature soft machines. *Nat. Commun.* **13**, 7919 (2022).
20. Fan, X., Sun, M., Sun, L. & Xie, H. Ferrofluid Droplets as Liquid Microrobots with Multiple Deformabilities. *Adv. Funct. Mater.* **30**, 2000138 (2020).
21. Katsikis, G., Cybulski, J. S. & Prakash, M. Synchronous universal droplet logic and control. *Nat. Phys.* **11**, 588–596 (2015).
22. Chaves, A., Zahn, M. & Rinaldi, C. Spin-up flow of ferrofluids: Asymptotic theory and experimental measurements. *Phys.Fluids*, **20**, (2008).
23. Rosensweig, R. E., Popplewell, J. & Johnston, R. J. Magnetic fluid motion in rotating field. *J. Magn. Magn. Mater.* **85**, 171–180 (1990).
24. Rosensweig, R. E. *Ferrohydrodynamics*. Courier Corporation, (2013).
25. Oron, A., Davis, S. H. & Bankoff, S. G. Long-scale evolution of thin liquid films. *Rev. Mod. Phys.* **69**, 931–980 (1997).
26. Kirkinis, E. & Davis, S. H. Hydrodynamic theory of liquid slippage on a solid substrate near a moving contact line. *Phys. Rev. Lett.* **110**, 234503 (2013).
27. Kirkinis, E. & Davis, S. H. Moffatt vortices induced by the motion of a contact line. *J. Fluid Mech.* **746**, R3 (2014).
28. Manukyan, S. & Schneider, M. Experimental investigation of wetting with magnetic fluids. *Langmuir* **32**, 5135–5140 (2016).
29. Latikka, M., Backholm, M., Timonen, J. V. I. & Ras, R. H. A. Wetting of ferrofluids: Phenomena and control. *Curr. Opin. colloid interface Sci.* **36**, 118–129 (2018).
30. Deb, R., Sarma, B. & Dalal, A. Magnetowetting dynamics of sessile ferrofluid droplets: a review. *Soft Matter* **18**, 2287–2324 (2022).
31. Brunet, P., Eggers, J. & Deegan, R. D. Vibration-Induced Climbing of Drops. *Phys. Rev. Lett.* **99**, 144501 (2007).
32. Noblin, X., Kofman, R. & Celestini, F. Ratchetlike Motion of a Shaken Drop. *Phys. Rev. Lett.* **102**, 194504 (2009).
33. Zakinyan, A., Nechaeva, O. & Dikansky, Y. Motion of a deformable drop of magnetic fluid on a solid surface in a rotating magnetic field. *Exp. Therm. Fluid Sci.* **39**, 265–268 (2012).
34. Edalatpour, M., Eid, K. & Sommers, A. Ferrofluid droplet behavior on gradient surfaces inside a uniform magnetic field, *arXiv preprint*arXiv:1910.13917 (2019).
35. COMSOL Multiphysics® v. 6.1. www.comsol.com. COMSOL AB, Stockholm, Sweden.
36. Donea, J., Huerta, A., Ponthot, J.-Ph. & Rodríguez-Ferran, A. Arbitrary Lagrangian–Eulerian methods. In *Encycl. Comput. Mech.* (eds Stein, E., Borst, R. and Hughes, T. J. R.) (2004).
37. Cai, Z. & Song, Y. Implementing contact angle hysteresis in moving mesh-based two-phase flow numerical simulations. *ACS omega* **6**, 35711–35717 (2021).
38. de Gennes, P. G. Wetting: statics and dynamics. *Rev. Mod. Phys.* **57**, 827 (1985).
39. Dussan, E. B. On the spreading of liquids on solid surfaces: static and dynamic contact lines. *Annu. Rev. Fluid Mech.* **11**, 371–400 (1979).

Acknowledgements

This work was supported by, and made use of the shared facilities at, the University of Chicago Materials Research Science and Engineering Center, which is funded by National Science Foundation under award number DMR-2011854. We thank Chloe Lindeman at University of Chicago for helping us to use the Krüss drop shape analyzer (DSA100).

Author contributions

A.A. and S-Y.C. contributed equally. A.A. developed the theoretical framework and designed the finite element analysis model. S-Y.C. carried out the experiments. A.A., E.K., S-Y.C., M.M.D and M.O.d.I.C. analyzed the data. A.A., S-Y.C., M.O.d.I.C., and E.K. wrote the manuscript. M.I.K and B.F. synthesised the hydrophobic glass plates used in the experiments. M.M.D and M.O.d.I.C directed the research.

Competing interests

The authors declare no competing interests.

Additional information

Supplementary information The online version contains supplementary material available at https://doi.org/10.1038/s42005-024-01871-8.

Correspondence and requests for materials should be addressed to Monica Olvera de la Cruz.

Peer review information *Communications Physics* thanks the anonymous reviewers for their contribution to the peer review of this work. A peer review file is available.